

## PONDER - A Real time software backend for pulsar and IPS observations at the Ooty Radio Telescope

Arun Naidu · Bhal Chandra Joshi · P.K  
Manoharan · M. A. Krishnakumar

Accepted by Experimental Astronomy

**Abstract** This paper describes a new real-time versatile backend, the Pulsar Ooty Radio Telescope New Digital Efficient Receiver (PONDER), which has been designed to operate along with the legacy analog system of the Ooty Radio Telescope (ORT). PONDER makes use of the current state of the art computing hardware, a Graphical Processing Unit (GPU) and sufficiently large disk storage to support high time resolution real-time data of pulsar observations, obtained by coherent dedispersion over a bandpass of 16 MHz. Four different modes for pulsar observations are implemented in PONDER to provide standard reduced data products, such as time-stamped integrated profiles and dedispersed time series, allowing faster avenues to scientific results for a variety of pulsar studies. Additionally, PONDER also supports general modes of interplanetary scintillation (IPS) measurements and very long baseline in-

---

Arun Naidu  
National Centre for Radio Astrophysics, Tata Institute of Fundamental Research, Pune 411  
007, India  
Tel.: +91 020 25719230  
E-mail: arun@ncra.tifr.res.in

Bhal Chandra Joshi  
National Centre for Radio Astrophysics, Tata Institute of Fundamental Research, Pune 411  
007, India  
Tel.: +91 020 25719244  
E-mail: bcj@ncra.tifr.res.in

P.K Manoharan  
Radio Astronomy Centre, National Centre for Radio Astrophysics, Tata Institute of Funda-  
mental Research, Udthagamandalam (Ooty) 643001, India  
Tel.: +91 0423 2244962  
E-mail: mano@ncra.tifr.res.in

M. A. Krishnakumar  
Radio Astronomy Centre, National Centre for Radio Astrophysics, Tata Institute of Funda-  
mental Research, Udthagamandalam (Ooty) 643001, India  
Tel.: +91 0423 2244959  
E-mail: kkma@ncra.tifr.res.in

terferometry data recording. The IPS mode yields a single polarisation correlated time series of solar wind scintillation over a bandwidth of about four times larger (16 MHz) than that of the legacy system as well as its fluctuation spectrum with high temporal and frequency resolutions. The key point is that all the above modes operate in real time. This paper presents the design aspects of PONDER and outlines the design methodology for future similar backends. It also explains the principal operations of PONDER, illustrates its capabilities for a variety of pulsar and IPS observations and demonstrates its usefulness for a variety of astrophysical studies using the high sensitivity of the ORT.

**PACS** 95.55.Ev · 95.55.Jz · 95.75.Wx · 96.50.Ci · 97.60.Gb

## 1 Introduction

Investigations of the pulsed emission from pulsars, which are rapidly rotating highly magnetized compact neutron stars, often require very high time resolution time-series data from a sensitive radio telescope, such as the Ooty Radio Telescope (ORT). The pulsed signal is dispersed by free electrons in the interstellar medium (ISM), causing the pulse to arrive at progressively later times with progressively decreasing frequencies. The degradation in time resolution and the signal-to-noise ratio (SNR) due to this effect can be compensated by the technique of coherent dedispersion (Hankins and Rickett 1975a), which is usually computationally intensive, particularly at low radio frequencies (below 400 MHz). A new real time software backend, Pulsar Ooty Radio Telescope New Digital Efficient Receiver (PONDER), implementing this technique in software using a Graphical Processing Unit (GPU) for pulsar observations is described in this paper. The new backend also enhances the quality of interplanetary scintillation (IPS) as well as incoherently dedispersed pulsar observations by providing standard data products in real-time.

Most pulsar studies require high time resolution data. Experiments involving tests of gravitational theories (Taylor and Weisberg 1989; Kramer 1998; van Straten et al 2001; Weisberg and Taylor 2002; Lyne et al 2004; Kramer et al 2006) and the detection of stochastic gravitational wave background using pulsar timing arrays (Foster and Backer 1990; Manchester et al 2013; Demorest et al 2013) demand a high degree of precision in measurements of the pulsar clock, which requires data sampled at fractions of micro-second. High time resolution studies of pulsars such as PSRs B0531+21 and B1937+21 reveal narrow intense highly polarized Giant Pulses (GPs), which provide constraints on the location and size of emission region as well as the emission mechanism (Sallmen and Backer 1995; Kinkhabwala and Thorsett 2000; Johnston and Romani 2002, 2003; Hankins et al 2003; Joshi et al 2004). Observations of microstructure, observed in pulsars such as PSRs B1133+16, B0950+08 and J0437–4715

(Jenet et al 1998; Popov et al 2002; Kramer et al 2002) place further constraints on the emission mechanism for pulsars. High time resolution observations also provide high precision astrometric measurements as illustrated by the distance measurement of PSR J0437–4715 system using annual-orbital parallax (van Straten et al 2001).

Traditionally, specialized hardware using Digital Signal Processing (DSP) or Field Programmable Gate Array (FPGA) chips were used to implement the coherent dedispersion algorithms. In recent years, the availability of inexpensive computers has allowed implementation of these algorithms in backends, employing clusters of computers, e.g. pulsar observing systems at Jodrell Bank, Giant Meterwave Radio Telescope, Westerbok, Arecibo, Parkes and Green Bank Observatories (Joshi et al 2003; Joshi and Ramakrishna 2006; DuPlain et al 2008; Karuppusamy et al 2008). A more suitable alternative is now provided by GPUs, primarily developed for gaming and with several thousand on-board processor cores. These can meet the high computational demands of coherent dedispersion, particularly at frequencies below 400 MHz, allowing on-line coherent dedispersion using a single personal computer (PC). PONDER employs a GPU for this purpose.

PONDER was designed to provide capabilities for high time resolution observations with the ORT, which is an offset parabolic cylindrical antenna, used as a sensitive single dish telescope for monitoring pulsars and the solar wind. Previous pulsar studies with the ORT were performed with 9 MHz of bandwidth with typical time resolution of about 128  $\mu$ s. Daytime observing at the ORT is allotted to the IPS studies, which are aimed at the regular monitoring of the solar wind over a wide area of the sky plane [e.g., Manoharan (2012)]. In the conventional IPS measurements, the intensity scintillation over a 4 MHz bandwidth obtained with the central beam of the correlated-beam system was recorded at a sampling interval of 20 ms (Manoharan et al 2001). In addition, it is proposed to use the ORT for Very Long Baseline Interferometry (VLBI) observations with telescopes in Russia, which also require Nyquist sampled voltage data at a very high time resolution.

The traditional approach for such observations has been high speed recording of the data followed by off-line analysis in the software due to the large computational resources required for analysis, particularly for large bandwidths. With the computational power available in PC and GPU boards, the routine off-line analysis can be done in real-time. This makes available real-time standard data products, several orders of magnitude smaller in volume than the raw data and simplifies their archiving. The software approach also increases the upgradeability and flexibility of the backend as new data products can be added in future with the underlying hardware replaced by ever improving computational machines available. In addition to the real-time coherent dedispersion capability, the design of PONDER was also partly motivated by these considerations.

The organization of the paper is as follows. A brief description of the ORT is presented in Section 2. The description of the hardware (Section 3.1) is followed by a discussion of the main design considerations of PONDER software (Section 3.2) and the required software pipelines (Section 3.3). The results of test observations, demonstrating the capabilities of the instrument, are presented in Section 4. Finally, a summary, with the possible future development, is provided in Section 5.

## 2 The Ooty Radio Telescope

The ORT is an offset parabolic cylindrical antenna, 530 m long in north-south direction and 30 m wide in east-west direction, with an effective collecting area of approximately 8500 m<sup>2</sup>. It is erected on a north-south mountain slope with an inclination equal to Ooty's geographical latitude (+11°23'), making it an equatorially mounted antenna with its long axis parallel to the earth's rotation axis (Swarup et al 1971). The radio waves reflected by the cylindrical reflector are received by an array of 1056 dipoles located along the focal line in north-south direction. Consequently, the telescope is sensitive to a single linear polarisation. This array is divided into 22 sub-arrays, called modules, with 48 dipoles each, which are phased to form module beams. These are themselves phased to a given declination, using electronic phase-shifters, before combining the signals of all modules, allowing the overall beam to be steered over a declination range of  $-57^\circ$  to  $+60^\circ$ . The telescope beam is steered in the East-West (hour-angle) direction by mechanical rotation of the antenna around its long axis. The signal from individual dipoles and modules are combined by a Christmas Tree network as is illustrated in Fig. 1. Each module output is mixed with a local oscillator of 296.5 MHz to obtain an intermediate frequency (IF) bandpass of 16 MHz centered at 30 MHz. Different fixed delays are used to synthesize 12 beams in the sky. The instrument described in this paper used one of the beams of the telescope, i.e., the central beam (Beam 7). The gain of the antenna is 3.3 K/Jy and the system temperature is 150 K.

## 3 Design of PONDER

PONDER has been designed to support four main modes: (i) a real time pulsar observing mode with filterbank, incoherent dedispersion and folded profile data products, (ii) a real time coherent dedispersion mode up to a maximum DM of 130 pc cm<sup>-3</sup>, (iii) a real time IPS mode with a bandwidth of 16 MHz and (iv) a baseband recorder mode for VLBI observations. The hardware architecture, design considerations and the software architecture of PONDER is described in the following sections.

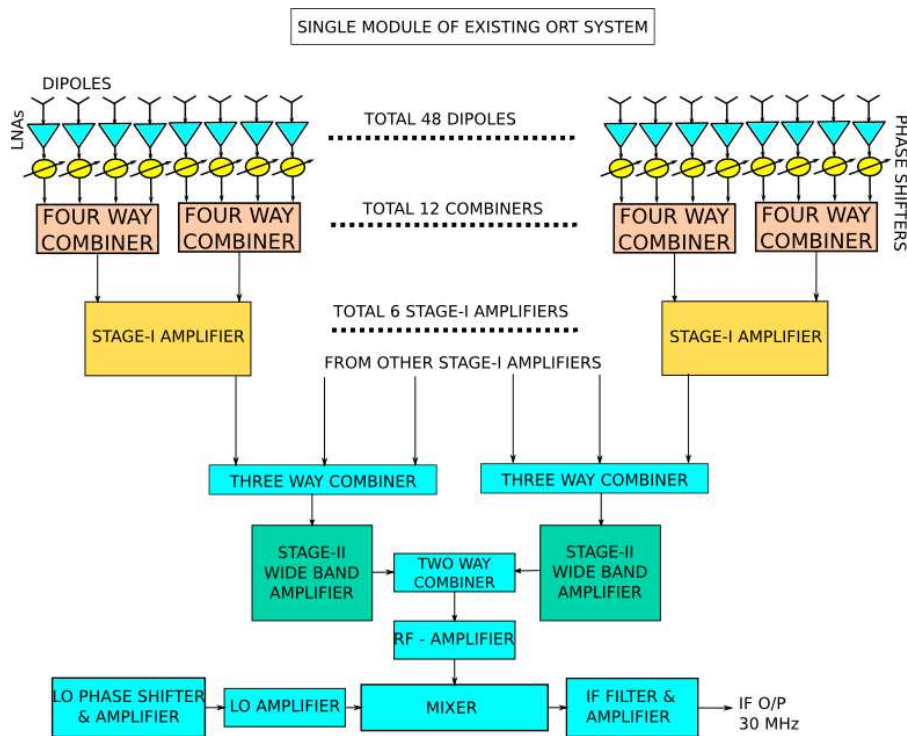


**Fig. 1** Block diagram of single ORT module consisting of 48 dipoles.

### 3.1 Hardware architecture of PONDER

The hardware architecture of PONDER is shown in Fig. 2. The 30-MHz IF output of Beam 7 of each half of the ORT is first amplified by a 30 dB amplifier and then mixed with a 38-MHz tone, generated using a frequency synthesizer locked to 10-MHz reference signal from a Rubidium oscillator disciplined by a Global Positioning System (GPS). The down-converted signal is recovered with a 16-MHz low pass filter. The power levels at the output of the filter can be suitably adjusted with variable gain attenuators before digitization using analog to digital converter (ADC). The signals from the two halves of the ORT are treated identically.

The filtered and down-converted outputs of the two halves of the ORT are digitized using a two channel Spectrum M3i.2122 ADC board mounted on a Peripheral Connect Interface (PCI) slot in a Xeon dual processor workstation server. This card has 8-bit resolution with values ranging from -128 to 127. The maximum possible sampling rate the ADC can perform is 250 MHz for both the channels and 500 MHz for single channel. The card has a provision for locking its sampling clock to an external reference clock, which was derived from the 10-MHz reference of a rubidium clock. The sampling clock can be

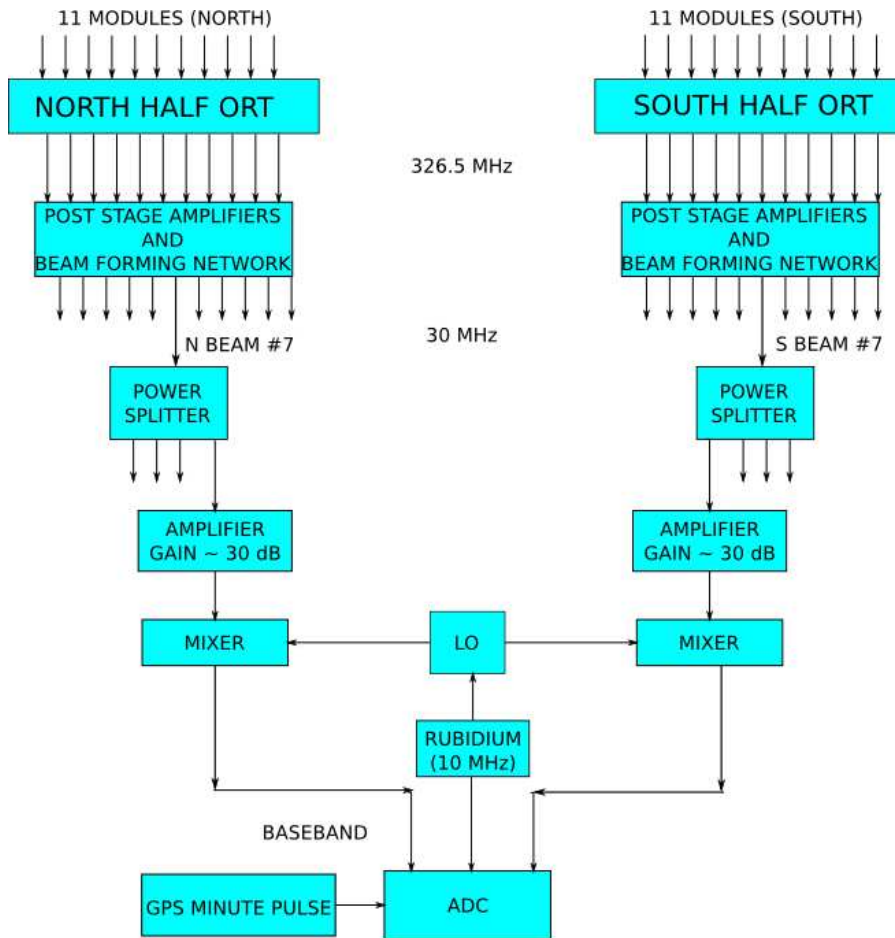


Fig. 2 Hardware architecture of PONDER.

varied from 30 MHz to 200 MHz. The observatory is equipped with GPS, which provides a pulse every minute with the pulse edge synchronized to 100 ns accuracy with the Universal Coordinated Time (UTC) and this was used to trigger the data acquisition by the ADC board. Thus, the time of the first sample of the time series is known to an accuracy of 100 ns. The ADC has an on-board memory of 1 GB to buffer the acquired data, which is streamed to the Random Access Memory (RAM) of the host workstation server without any data loss up to 240 million samples per second.

Based on benchmark tests, carried out on different available host PC configurations (as of 2012), a low-cost configuration satisfying the requirements for all modes, except the coherent dedispersion mode, was selected. The host used for the digitizer is a server with dual Intel Xeon E5645 processors clocked at 2.4 GHz with 6 cores each. There is 32 KB of on-chip L1 data cache per core, 256

KB L2 cache per core, and 12 MB of shared L3 cache. The server was equipped with 32 GB of RAM and 9.5 TB of available storage space. The theoretical peak performance of the system is 230 Gflops<sup>1</sup>, in single precision. Parallel processing can be performed using the 12 cores with two way hyperthreading. In the case of PONDER, the hyper threading was disabled because the number of the physical cores were more than the number of threads required for software implementation.

The server is also equipped with an NVIDIA Tesla K20C with a GK110 GPU, with 2496 processing cores, arranged in units of 192 streaming multiprocessor (SM) and an on-board 5012 MB Graphics Double Data Rate, version 5 (GDDR5) memory with a bandwidth of 5 GB/s. Each multi-processor has 65536 32-bit floating point registers and 32 KB of shared memory. The theoretical single precision performance of the GPU is 3.5 Tflops and double precision performance is 1.17 Tflops<sup>2</sup>. The GPU sits on a full length x16 PCI express slot in the host machine.

### 3.2 Design considerations

The salient tasks for real time operation are (i) data acquisition, (ii) data transfer to host PC-RAM, (iii) Fast Fourier transform (FFT) operation on the data to synthesize a digital filterbank, (iv) correlation, integration, dedispersion/computation of fluctuation spectra, and (v) transfer of processed data from RAM to host hard disks. Nyquist sampling of 16 MHz band from the two halves of the ORT implies a data acquisition speed of 64 M-samples per second, which has to be reduced to the final data products and recorded in less than a second for a real time capability. The execution time for the required tasks in a serial fashion, computed using our benchmark codes, is about 3.8 times the time required for data digitization for modes other than coherent dedispersion mode and even larger for coherent dedispersion. Hence, to achieve the real time computation, parallel computing is required.

Our tests indicated that the FFT, involved in the digital filterbank or coherent dedispersion, take the largest execution time. The execution time of a FFT is a function of its length,  $N$ , which depends on the frequency of observations ( $f_h$ ), the bandwidth ( $\delta f$ ), sampling time ( $ts$ ) and the dispersion measure<sup>3</sup> ( $DM$ ) and is given by the following expression

$$N = \frac{2}{(f_h - \delta f)^2} - \frac{2}{f_h^2} \times \frac{DM}{2.41 \times 10^{-4} \times ts} \quad (1)$$

<sup>1</sup> <http://ark.intel.com/products/48768/Intel-Xeon-Processor-E5645>

<sup>2</sup> <http://www.nvidia.com/object/tesla-servers.html>

<sup>3</sup> The dispersion measure is the measure of column density of free electrons integrated over the line of sight to the pulsar, expressed in units of  $\text{pc cm}^{-3}$

We used both publicly available benchmark codes, such as *benchfft*<sup>4</sup>, with FFT implemented in publicly available Fastest Fourier Transform in the West (FFTW) libraries<sup>5</sup>, as well as a benchmark code developed by us<sup>6</sup>, which calculates the execution times separately for constant data volume as well as constant number of floating points. In particular, the benchmark with constant floating points was developed by us to get an estimate of the execution times independent of the length of FFT. These codes were also implemented for GPU using the GPU programming platform Compute Unified Device Architecture<sup>7</sup> (CUDA) and CUDA C and CUFFT<sup>8</sup>. These benchmarks are useful to explore the effects of different cache sizes on the execution times of the slowest FFT steps in all modes.

PONDER software was sub-divided into tasks, which were run parallelly (task parallelism) in different threads. The results of our benchmark tests were used in the design of the software architecture to balance the computation load with suitable task parallelism for all modes of PONDER. While task parallelism is adequate for all modes other than the coherent dedispersion mode, the computation load for this mode is dominated by FFT required for dedispersion and is much larger than the time required for data digitization. For example, observations of a pulsar with a DM of  $130 \text{ pc cm}^{-3}$  with the proposed backend, the length of FFT is about 135 million points ( $2^{27}$  points). Hence, data parallelism (single instruction multiple data) amongst multiple cores in GPU was used for this mode. The benchmark tests on GPU showed that the FFT was performed about 30 times faster than on general purpose CPU for 32768 point FFT and the speed-up was much larger for longer FFT lengths.

### 3.3 Software architecture of PONDER

Broadly, the software architecture is divided in two main processes a) ADC process (process I) and b) data reduction and recording process (process II). The Process I is run as root and process II runs as user. The real time processing requirement of the receiver are met by inter-process communication (IPC) implemented with shared memory and task parallelism using POSIX threads. These are implemented using the *pthread* library, which is available on all modern UNIX systems. The communication between the two main processes is achieved using shared memory and is protected by another IPC device, namely the semaphores, to achieve synchronization between the processes. Mutexes are used for synchronization between threads. All the FFT operations, implemented on the host server workstation with dual Intel Xeon E5645 processors, used the FFTW library. The receiver also uses CUDA API developed by NVIDIA. The PONDER software implements the four primary modes

<sup>4</sup> <http://www.fftw.org/benchfft>

<sup>5</sup> <http://www.fftw.org/>

<sup>6</sup> <http://ponderpulsar.sourceforge.net>

<sup>7</sup> CUDA is a trademark of NVIDIA Corporations

<sup>8</sup> <http://docs.nvidia.com/cuda/cufft>

of operation of the backend as mentioned in the beginning of Section 3. The structure of the software and its operation for each of the major modes of operation of PONDER are described in detail in the following sections.

### 3.4 Real-time pulsar mode with incoherent dedispersion

In this mode, PONDER is used for pulsar observations with incoherent dedispersion. This is the simplest way to compensate for the effects of pulse dispersion due to the ISM. This method involves splitting the incoming frequency band into narrow channels. The voltage in each channel is then converted to power and consequently the phase information is lost. The signal in each channel therefore suffers from a residual dispersive delay given by

$$\Delta t_{res} \simeq 8.3 \times 10^6 \frac{\Delta f_{ch} \times DM}{f_{ch}^3} \text{ (ms)} \quad (2)$$

where,  $f_{ch}$  is the frequency in MHz corresponding to the channel,  $\Delta f_{ch}$  is the bandwidth in MHz per channel. The effective time resolution of this mode therefore depends on DM (in  $\text{pc-cm}^{-3}$ ) and the bandwidth per channel and is worse than that achievable with coherent dedispersion. For large DM pulsars, the limit on time resolution is in any case set by scatter-broadening, which increases approximately with the second power of DM (Romani et al 1986). The scatter-broadening for these pulsars is much larger (typically greater than 4 ms) than the corresponding dispersion smear for 1024 channels across 16 MHz bandpass ( $3.8 \mu\text{s}/\text{DM pc-cm}^{-3}$ ). For such pulsars, the excessive computation required by the coherent dedispersion mode is not necessary and the incoherent dedispersion is sufficient.

In the incoherent dedispersion mode, appropriate time delays, given in Eq. 3, are applied to the detected signal in each channel to compensate for the dispersive delay across channels.

$$\Delta t_{DM} \simeq 4.15 \times 10^6 (f_{ref}^{-2} - f_{chan}^{-2}) \times DM \text{ (ms)} \quad (3)$$

where  $f_{ref}$  is the reference frequency of the bandpass of the receiver and  $f_{chan}$  is the frequency corresponding to channel under consideration (both frequencies expressed in MHz). In this mode, there are two different sub-modes to select: (i) Adding Incoherent Dedispersion (AID) mode and (ii) Correlation Incoherent Dedispersion (CID) mode. In the former, the digitized data from the two halves of the ORT are added in phase before dedispersion, whereas in CID mode, the data from both the channels are correlated before performing dedispersion. While AID mode provides  $\sqrt{2}$  better sensitivity than CID mode, the latter is less prone to radio frequency interference (RFI) as the RFI picked in one half of the ORT will in general not be correlated with that in the other half. Figures 3 and 4 show how these two sub-modes are implemented. All the threads are shown in blue and the shared memory is shown in yellow.

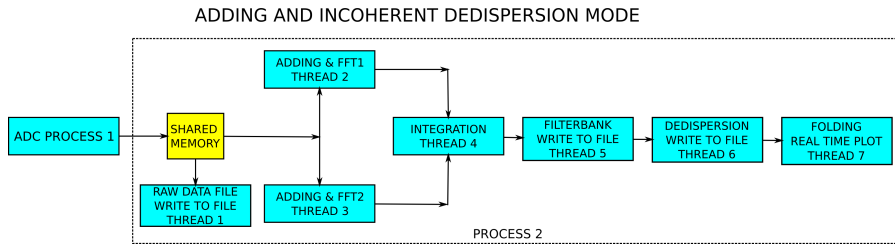


**Fig. 3** Flow chart showing the Adding in Phase and Incoherent dedispersion mode (AID). All the tasks in process 2, indicated by a dashed box, are implemented in concurrently running threads labeled by thread number for reference in the text. The threads and processes are shown in blue color and the shared memory in yellow.

### 3.4.1 Adding and Incoherent dedispersion mode(AID)

In this mode, all the threads shown in the Fig. 3, are executed. The pipeline was designed with different tasks distributed over the minimum required number of threads to achieve a balanced computation load. Each process/thread is executed on a different core/processor of the host PC. The data from the process I are passed on to two threads (threads 2 and 3) of process II. Successive blocks of 128 MB are directed to threads 2 and 3 alternately by process I. These are also passed to thread 1 for a record of raw data. In the threads 2 and 3, the data are added in phase and FFT is performed using the FFTW library. Two concurrent threads were used for addition and FFT as the compute to observed ratio (COR)<sup>9</sup> for a single thread exceeded 1. The resultant spectra are passed onto the next thread (4), where each spectra is squared to get power and added to achieve the desired temporal resolution. These power spectra are passed on to the filterbank thread (5), where they are converted into SIGPROC<sup>10</sup> filterbank format. The filterbank thread writes the data in this format to the hard-drive and forwards it to the dedispersion thread (6), where it is incoherently dedispersed to a user specified DM and written to a file as binary data with an appropriate SIGPROC header. The dedispersed time series from this thread is folded with appropriate period, obtained from the TEMPO2 predictors (Hobbs et al 2006) by the fold thread (7). The folded profile is generated in real-time and written periodically to disk and is displayed on the screen by the Graphical User Interface (GUI). The final average profile produced by the fold thread is written as an ASCII file. While the output of the dedispersion and fold threads is compatible with SIGPROC time series and profile format, the code for these threads was developed independently by us. The tasks are distributed to the seven threads so that the execution time for each is less than the data digitization time (COR < 1.0).

The filterbank data, dedispersed time series and folded profiles are written with SIGPROC headers (Lorimer 2001), which contain essential information

<sup>9</sup> the ratio of the execution time of a thread to the data digitization time, which should be less than 1 for real-time capability

<sup>10</sup> [www.sigproc.sourceforge.net](http://www.sigproc.sourceforge.net)

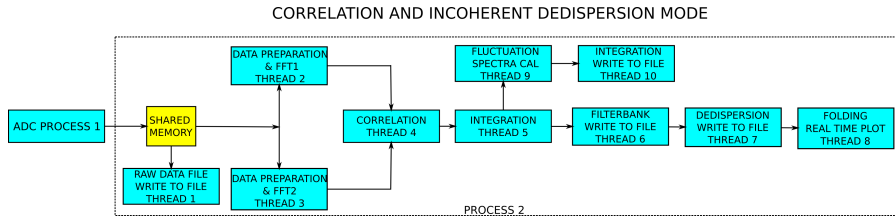


**Fig. 4** Flow chart for the correlation and Incoherent dedispersion mode (CID) and IPS mode. All the tasks in process 2, indicated by a dashed box, are implemented in concurrently running threads labeled by thread number for reference in the text. The threads and processes are shown in blue color and the shared memory in yellow.

about the observations such as the modified Julian date (MJD) of observations, the frequency of observations, bandwidth per channel, total duration of observations, nominal DM and period. The software allows either a simultaneous recording of raw data, filterbank data, dedispersed time series and folded profiles or a recording of selected data products out of these based on the parameters supplied by the user through GUI.

### 3.4.2 Correlation and Incoherent dedispersion mode (CID)

In this mode, all threads in process II (Fig. 4) other than threads 9 and 10 (required for IPS mode) are used. The data passed on by process I through the shared memory are first sorted into two individual channels representing the two halves of the ORT in threads 2 and 3. Then, the FFT is performed on the data from individual halves by these threads. Two concurrent threads are required for these operations as the COR for a single thread exceeded 1. The spectra of North and South halves, obtained respectively by threads 2 and 3, are then correlated by thread 4 by multiplication of the North and South spectra. The correlated spectra are accumulated up to user specified integration time by integration thread (5). The rest of the operation of this mode is similar to that of AID mode and is handled in a similar fashion by threads 6 to 8. The tasks were distributed to the eight threads used so that each has a COR much less than 1.

Both the above modes perform incoherent dedispersion. The performance of incoherent dedispersion program as a function of bandwidth is plotted in Fig. 5. As the sampling frequency is increased, the ratio of processing time to real time increases. Since CID is more computationally intensive, the increase is much steeper. The COR for AID is less than 1 until 45 MHz, while CID can operate until 25 MHz with a COR of less than unity. For the current 16 MHz system, both modes operate in real-time. This shows the longevity of the receiver if the bandwidth is increased in future upgrade to ORT.

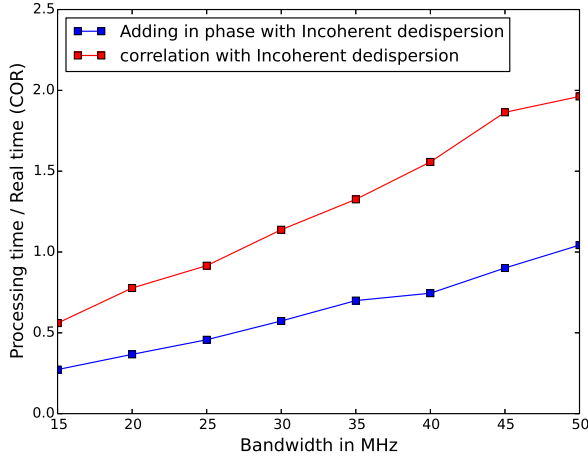


**Fig. 5** The ratio of processing time to real time for AID and CID modes. The mode can run in real time if the value is less than 0.9.

### 3.5 Inter planetary scintillation mode (IPSM)

The flexibility of the data acquisition of the PONDER system has motivated us to initiate an interplanetary scintillation mode, which provides observation over a wider bandwidth (16 MHz) than the legacy system currently in use at the ORT. In this mode, threads 2 to 5 and 9 to 10 of process II ( Fig. 4) are used. The data from the process I are passed on to threads 2 and 3 of process II. The processing for IPS is similar to CID mode of pulsar observations and is carried out by threads 2 to 5, where the data from the two halves of the ORT are correlated after performing FFT and the cross spectra thus obtained are integrated up to a user specified integration time (typically  $\sim 1$  ms). The intensity scintillation time series obtained from the PONDER can support a time resolution starting from  $64 \mu\text{s}$  or higher. The integrated spectra are collapsed and the resultant time-series is written to hard disk by thread 9 for offline analysis.

The data processing of the IPS signal primarily involves obtaining the temporal power spectrum of the intensity collapsed scintillation time series. The temporal spectrum of a given scintillating radio source is computed for the required frequency range and resolution, i.e., by appropriately choosing the sampling rate and the length of the data. In the real-time operation, the collapsed scintillation time series is further integrated to the required time resolution followed by computation of its fluctuation spectra over appropriate length of data by thread 10 by performing suitable length FFT. These spectra can further be accumulated to improve signal-to-noise ratio. The accumulated spectra are written as final data product by this thread.

### 3.6 VLBI/raw data mode of PONDER

PONDER can be used as a baseband data recorder. This mode of operation is primarily useful for VLBI observations, but is also useful for developing an offline pipeline for any astrophysical investigation not covered by the current functionality of PONDER. In this mode, only the process I and thread 1 of process II are used (see Fig. 3). The baseband input from the two halves of the telescope are digitized by the ADC in process I. Each 128 MB block of data contains samples from both channels arranged in an interleaved fashion. This block is transferred to thread 1 of process II. This thread can be configured to write the raw data as it is to a file on hard disk or to convert it into standard VLBI format. The VLBI format currently implemented is Mark 5B<sup>11</sup>.

### 3.7 Phase-coherent dedispersion mode for pulsar observations (PCD)

Phase-coherent dedispersion completely removes the dispersive effects of ISM, which can be described as a cold, tenuous plasma. The frequency response function resembles a unity-gain phase delay filter (Eq. 4) and its inverse is used to deconvolve the observed signal (Hankins 1971; Hankins and Rickett 1975b).

$$H(f + f_0) = \exp\left(i \frac{8.3 \times 10^3 \times \pi DM f^2}{f_0^2(f + f_0)}\right) \quad (4)$$

Here  $f_0$  is the center frequency of the observed band and all frequencies are expressed in MHz. DM is given in  $\text{pc-cm}^{-3}$ .

While the required filtering operation can be done as a convolution in the time domain, it is more efficient to perform this in the frequency domain, where the observed signal is simply multiplied with the discrete form of inverse of the frequency response function ( $H^{-1}$ ) along-with an appropriate taper function, which is required to take care of sample to sample leakage in an FFT with square window. The length of the impulse response of the filter in Eq. 4 has to be larger than the dispersion smear and has to also take into account the edge effects in a cyclical convolution. For a typical DM of  $130 \text{ pc cm}^{-3}$  at the ORT observing frequency of 326.5 MHz, this length is about  $2^{27}$ . While such long FFTs are difficult to execute on the host server with Xeon processor for 16 MHz bandwidth, these can be easily implemented on a GPU using CUDA C.

The CUDA C program consists of both host (CPU) and device (GPU) code. So a traditional C compiler will not accept the code. The code need to be compiled by a compiler that recognizes and understands both host and device code. We used CUDA C compiler by NVIDIA called NVIDIA C COMPILER

<sup>11</sup> <http://www.haystack.edu/tech/vlbi/mark5/>

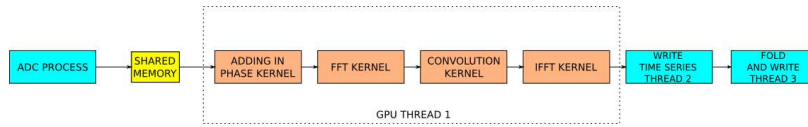


**Fig. 6** Signal flow diagram showing coherent dedispersion. All the blocks in orange are kernels. The GPU thread in process II is indicated by dotted box around the kernels.

(NVCC). NVCC processes a CUDA program using CUDA keywords to separate the host code with the device code. The device code is marked with CUDA keywords for labeling data-parallel functions, called kernels, and their associated data structures. Each CUDA kernel can execute a massive number of threads. All these threads run in parallel. The signal flow diagram for the implementation of coherent dedispersion on GPU is shown in the Fig. 6. The data stored in the host are sent to the GPU device (global memory) using shared memory. The GPU process consists of four kernels. The Adding in phase (AIP) kernel consists of  $2^{27}$  threads, where the interleaved data from both the halves of ORT are added in phase. After the AIP kernel, the data are passed through the FFT kernel, which performs the FFT using the CUFFT API. The resultant spectra are multiplied with the filter function  $H^{-1}$  by the convolution kernel. In GPU programming, the execution time is governed by the number of global memory accesses (GMA) performed by each thread. In the convolution stage, each thread requires corresponding FFT output value and corresponding chirp function value. The FFT output value is stored in the register memory of each thread and the chirp function value is calculated by each thread every time the kernel is executed, instead of storing the values in the global memory to maintain the GMA to 1. Finally, the filtered signal is converted to time domain in the IFFT kernel after applying the taper function. All the kernels are run in sequence and output of the IFFT kernel is sent to data output thread, where the dedispersed time series is written to the hard-drive using SIGPROC format. The last thread folds the dedispersed time series to the required number of bins and writes the folded profile to the hard-drive. The three threads in the process II run concurrently.

The performance of PONDER in PCD mode is shown in Fig. 7. The processing time to real time ratio is well below unity for the design bandwidth of 16 MHz, which shows that PONDER can routinely carry out coherent dedispersion at the ORT. The current limitation on  $N$  is due to the on board memory of 5 GB. In this case, it translates to  $2^{27}$  points. With this limitation in mind, the maximum DM that can be observed depends on the bandwidth and frequency of observation. The plots shown in Fig. 7 are independent of observing frequency. The maximum possible observable DM should be calculated from the observing frequency and bandwidth using Eq. 2. In the case of PONDER operating at 326.5 and 16 MHz bandwidth, this DM is  $130 \text{ pc cm}^{-3}$ . In actual practice, particularly for low latitude pulsars and pulsars towards the Galactic center, the time resolution is limited by the scatter-broadening of the pulse

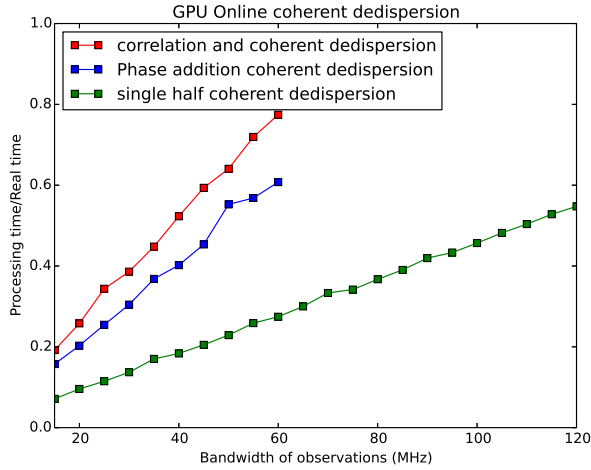


**Fig. 7** The ratio of processing time to real time as a function of bandwidth for different modes of coherent dedispersion at maximum possible DM. The mode can run in real time if the value is less than 0.9.  $N$  is  $2^{27}$  which determines the maximum DM. The red and blue curve show the COR for processing data from both halves of the ORT, whereas the green curve shows the COR for one half only.

**Table 1** Data products available for different modes

| Mode | Rawdata or VLBI | filterbank data | dedispersed data | real time folded profile | fluctuation spectra |
|------|-----------------|-----------------|------------------|--------------------------|---------------------|
| AID  | yes             | yes             | yes              | yes                      | no                  |
| CID  | yes             | yes             | yes              | yes                      | no                  |
| PCD  | yes             | no              | yes              | yes                      | no                  |
| IPS  | yes             | no              | no               | no                       | yes                 |

at 326.5 MHz to a much smaller DM value, as discussed in Section 3.4, and coherent dedispersion is not necessary except for studies of GPs and scatter-broadening by the ISM.

### 3.8 Graphical User Interface (GUI)

A Graphical User Interface (GUI) was developed, using Perl-Tk package, for user-friendly observations with PONDER. The GUI allows the user to customize and start the observations as per the user inputs and select the possible data products, listed in Table 1, for the desired mode. Three different types of observations can be customized by the user - (1) Individual source (pulsar) mode, (2) List mode and (3) IPS mode.

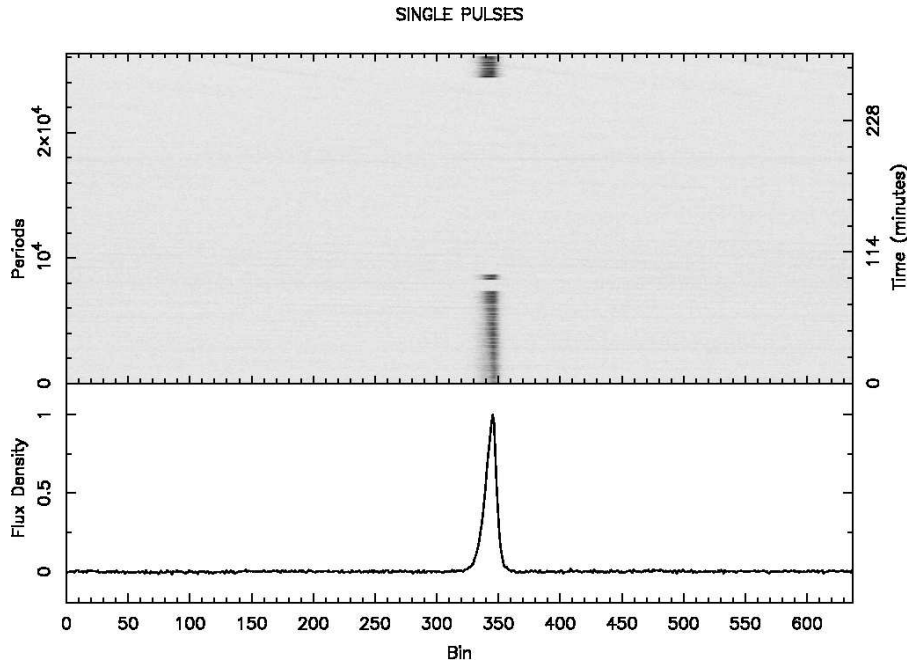


**Fig. 8** The top panel shows the gray scale single pulse plot of PSR J1709–1640 showing the long null observed using PONDER. The bottom panel is the corresponding integrated profile. The x-axis is in bins and the y-axis on left is in periods and on the right is in minutes. The arrival of the pulse at a constant phase (bin) indicates the stability of the system for long observations.

#### 4 Illustration of the capabilities of PONDER

PONDER was tested for different types of pulsar and solar wind observations after its implementation. A brief account of these test astronomical observations illustrating the capabilities of the instrument are highlighted in this section.

During tests, PONDER provided high quality time series on pulsars. The variation in single pulse energies for strong pulsars, such as PSR B0329+54, was useful to characterize saturation effects in the backend and devise strategies to alleviate such effects, particularly for strong single pulses, such as Giant pulses. With 8-bit digitization, the receiver also has high dynamic range, useful for fluctuation studies as well as modulation index studies.

Fig. 8 shows a single pulse plot of 26265 pulses of PSR J1709–1640 ( $P=0.653$  s,  $DM=24.87$  pc cm $^{-3}$ ) observed over 4.8 hours, illustrating the long term stability of PONDER, useful for long monitoring observations of such pulsars with interesting single pulse behaviour. A clear cessation of emission for more than 2 hours is seen, which suggests prominent long nulls in this pulsar. With

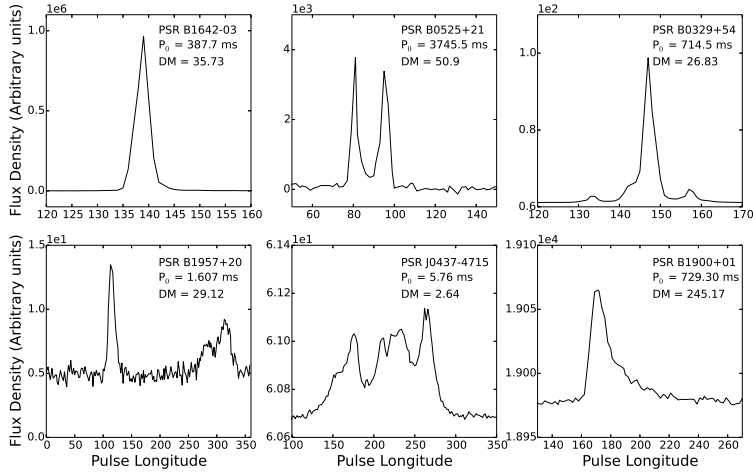


**Fig. 9** This figure shows the integrated profiles of a few pulsars, with a range of periods and DMs, observed during the test runs with PONDER. The flux density in arbitrary units is plotted against pulse longitude in degrees (one period =  $360^{\circ}$  degrees), for appropriately selected longitude range, where the pulsed emission is seen, in each panel. The pulsar name, period and DM are given in the top left corner of each panel.

its capability of real time dedispersion, even at high time resolution, such long observations do not require large storage space and can be analyzed quickly allowing studies of pulsars with interesting behaviour. In addition, these real-time single pulse plots, together with integrated profiles, can be used to assess data quality, while the simultaneous recording of raw data in SIGPROC filterbank files helps in a more refined off-line analysis.

Radio pulsars, with periods ranging from 1.57 ms to 3.74 s and DMs ranging from 2.64 to  $439 \text{ pc cm}^{-3}$ , have been observed in order to test PONDER. A selection of integrated profiles from these test observations is shown in Fig. 9 and illustrates the variety of average emission studies that can be carried out using PONDER. Multi-epoch monitoring with PONDER of such profiles can be useful for pulsar timing and mode-changing studies. Repeatability of these profiles over several days is also a useful test of the stability of the backend. In the validation phase of PONDER, a set of pulsars was observed in frequent test observations. As these were test observations, the time-series and profiles were recorded with a coarse sampling time (about  $64 \mu\text{s}$  or more) in order to avoid excessive data volume. The repeatability of profiles is illustrated by the timing residuals for 7 pulsars, obtained using timing analysis software TEMPO2, from such multi-epoch test observations (Fig. 10). While these test data are useful for validating the repeatability of profiles, it must be noted that these tests were not intended as high precision timing observations. Nevertheless, peak to peak variation in these residuals range from  $260 \mu\text{s}$  to 12 ms (root-

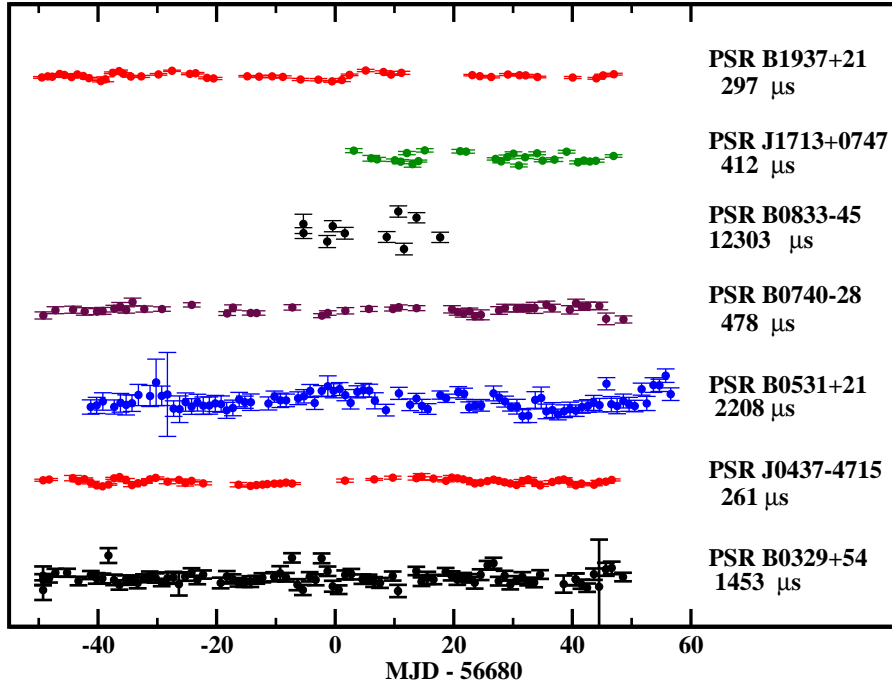


**Fig. 10** The timing residuals for 7 pulsars observed over 100 days. These residuals were obtained after subtracting barycentre corrected times-of-arrival of the pulses from those predicted using the known rotational model of each pulsar. The name of pulsar and peak-to-peak amplitude of the residuals is indicated on the right hand side of the plot.

mean-square residuals of about  $50 \mu\text{s}$ ) over about 100 days demonstrating the stability of instrument as well as its capability for routine pulsar timing observations for large pulsar timing experiments. In case of PSR J0437–4715, relatively larger residuals, despite its high SNR profile, are probably due to profile changes that were observed. We believe that these could be due to Faraday rotation and the single polarisation nature of the data. Lastly, observations of a large sample of pulsars at low frequencies can provide estimates of scatter-broadening in ISM and results of such a study are described in a separate work (Krishnakumar et al 2015).

The fine structure of pulse emission can be better understood using high time resolution data on a radio pulsar, which requires coherent dedispersion. As this was the main motivation for developing this system, we carried out high time resolution observations of several pulsars with real-time coherent dedispersion being performed on the GPU. The integrated profiles of two fast MSPs, PSRs B1937+21 ( $P = 1.5 \text{ ms}$ ,  $\text{DM} = 70 \text{ pc cm}^{-3}$ ) and B0531+21 ( $P = 33 \text{ ms}$ ,  $\text{DM} = 56.8 \text{ pc cm}^{-3}$ ), with a phase resolution integrated up to  $1 \mu\text{s}$  from the base resolution of  $62.5 \text{ ns}$ , are shown in Fig. 11. The profiles are scatter-broadened at  $325 \text{ MHz}$  as is evident from these figures. The use of incoherent

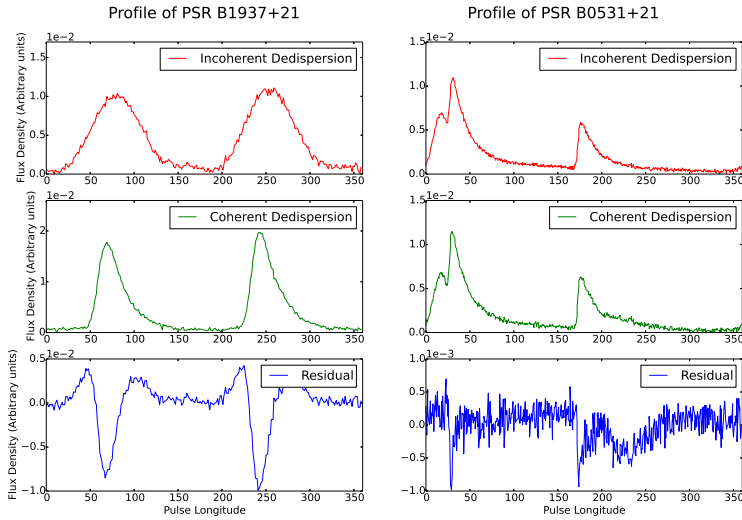


**Fig. 11** Comparison of profiles for pulsars PSR B1937+21 (left panels) and PSR B0531+21 (right panels) obtained after incoherent and coherent dedispersion. For each pulsar, the top panel shows the incoherently dedispersed integrated profile, the middle panel shows the coherently dedispersed integrated profile and the bottom panel shows the difference between the profiles in the top and middle panels. The flux density in arbitrary units is plotted against the pulse longitude in degrees in each panel.

dedispersion, even with 1024 channels, for these observations typically leaves a dispersion smear of  $3.8 \mu\text{s DM}^{-1}$ , which affects true scatter-broadening measurements for these pulsars (typical scatter-broadening tails of the order of 0.3 ms for PSR B1937+21). For low DM MSPs, generally used in pulsar timing array experiments, the high time resolution observations, made possible by PONDER, provide low post-fit residual times-of-arrival.

Sometimes, the dispersion smear due to incoherent dedispersion can hide pulse components or lead to a large uncertainty in estimating pulse separation or ratio of pulse components. Fig. 11 shows the average profile of PSR B0531+21, obtained with both incoherent and coherent dedispersion. The difference between these two profiles is also shown, which clearly indicates the result of dispersion smear. The scatter-broadening in this pulsar varies with time and sometimes can completely hide the precursor component (the component before the stronger of the three components) at this frequency as the main pulse and the precursor merge. Such observations with PONDER are useful to study the profile evolution of short period radio pulsars at lower frequencies.

Another area of investigations, where PONDER will be very useful, is the study of giant pulse (GP) emission and micro-structure. GPs are narrow pulses,

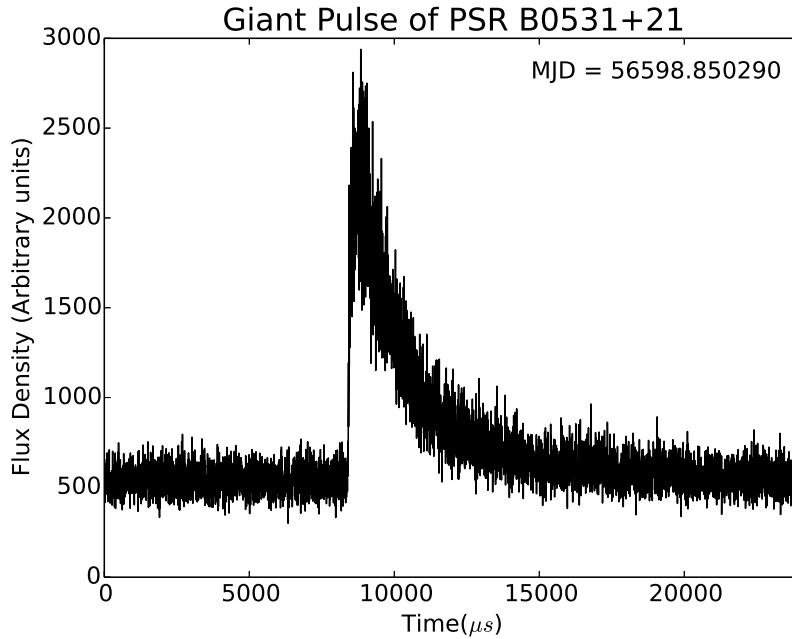


**Fig. 12** Plot of the Giant Pulse of PSR B0531+21 observed using PONDER at MJD 56598.850290. The flux density in arbitrary units is shown as a function of time. The time resolution is  $1 \mu\text{s}$ . The scatter-broadening tail is clearly visible.

with intensity several order of magnitude higher than the mean intensity, exhibited by a small number of pulsars (Lundgren et al 1995; Kinkhabwala and Thorsett 2000; Johnston and Romani 2003; Joshi et al 2004). GP emission is as yet not well understood. A GP in PSR B0531+21 observed using PONDER is shown in Fig. 12 with a time resolution of  $1 \mu\text{s}$ . As GPs are almost impulse like, pulsars with scatter broadened GPs can be useful in estimating the true scatter-broadening time scale in these line of sight.

Lastly, PONDER has been extensively tested during IPS observations. Simultaneous IPS measurements on a large number of scintillating radio sources using both PONDER and the old conventional 4-MHz correlated-beam system at the ORT were carried out. These observations covered a period of about two months, during February and April 2014. For observations on a radio source, the scintillation time series from the PONDER was integrated to 20 ms sampling to match the conventional system observing data rate. The time series from the above two systems have been processed using an identical analysis procedure to yield the temporal power spectra, covering a temporal frequency range of 0 to 25 Hz. In Fig. 13, some of the sample spectra obtained from PONDER (red color) and conventional system (green color) are displayed. In this figure, the scintillating power (in dB) is plotted as a function of loga-

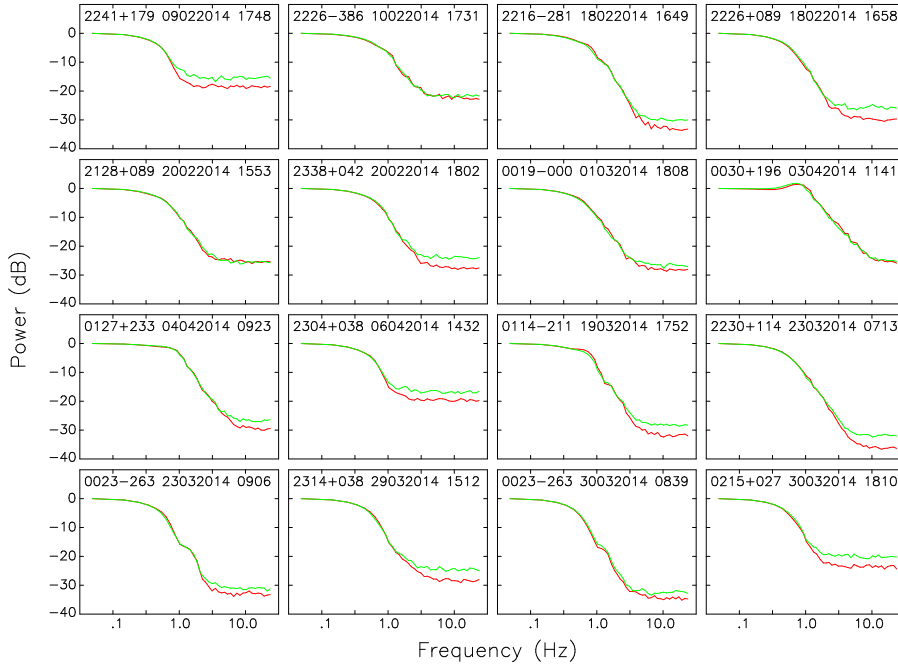


**Fig. 13** This figure shows spectra obtained from the old 4-MHz system (green color) and new PSR system (red color). The top legend on each small plot gives the source name (B1950), date and time of observation.

rithm of temporal frequency (Hz). In each spectral plot, the radio source name (in B1950 format), date and time of observation are shown at the top. It is evidently clear that the PONDER measurements reproduced each and every feature observed in the old conventional system. In particular, the spectra, obtained with PONDER, reproduces specific features in the declining part of the spectra, seen in the spectra obtained by the conventional system for 0030+196, 0114-211 and 0023-263. This essentially validates the IPS observing mode of PONDER.

It is interesting to note that for most of the spectra, the PONDER measurements provide an excess signal around 1 Hz frequency range of the spectra. In other words, the noise level of the PONDER system is lower than the old system. This is consistent with the increase in bandwidth from the old system of 4-MHz to a 16-MHz PONDER system. The increase in power spectrum signal is evident in Fig. 14, which shows the correlation plot of power spectrum signal observed between the old conventional 4-MHz system and the new 16-MHz PONDER system. This plot includes spectral signals of 364 simultaneous IPS observations made between the old and new systems. The dotted line indicates the one-to-one correlation line between two data sets. The continuous line is the best straight-line fit to the observations. On the average PONDER tends to give a 3dB increase in spectral power compared to the old system, which

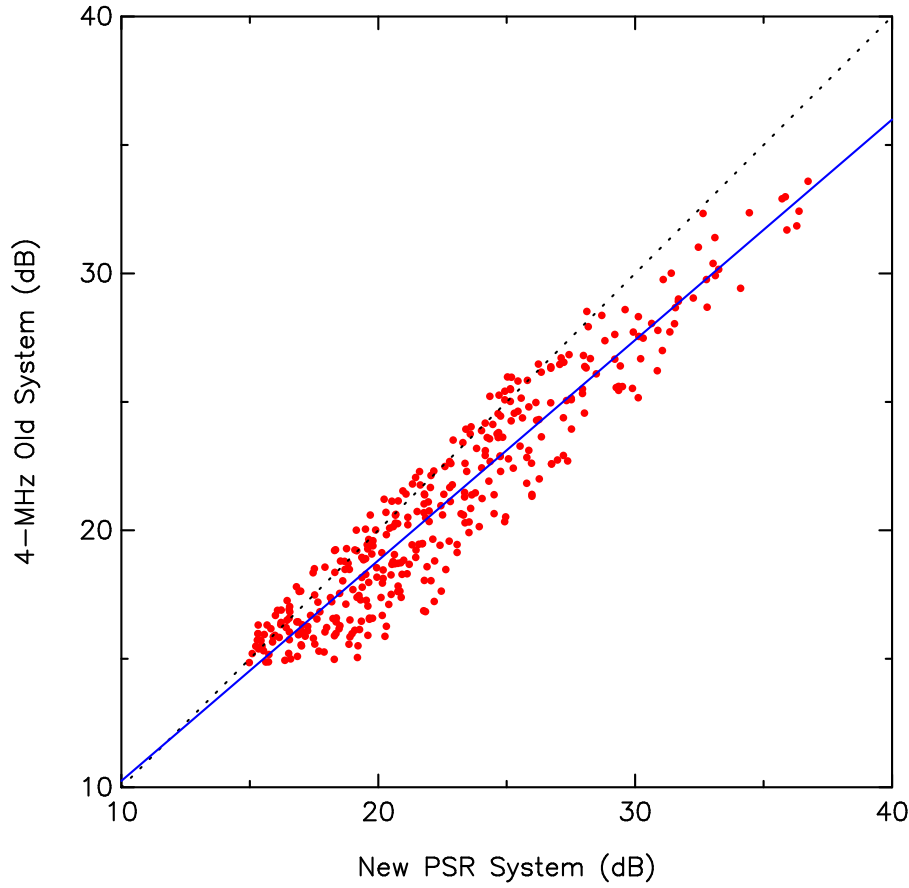


**Fig. 14** A comparison of the spectral power observed with the old 4-MHz system and the PONDER. The x and y-axis scales are in dB. The dotted line is the one-to-one correlation line. The solid line is the best fit to the data points. On the whole the PONDER gives higher S/N by 3 dB. One can see higher scatter towards low S/N side, implying that the points lying above the dotted line in this region are probably affected by higher RFI included in the wide bandwidth of the PONDER.

is in agreement with the increase of bandwidth by about 4 times. However, since the PONDER is a wide band system, it can include more RFI signals than that of the old 4-MHz system and this could be the likely reason for the larger scatter in this figure for the lower signal-to-noise ratio spectra (near 20 dB) observed with the PONDER. Nevertheless, the PONDER system gives an additional power at the high frequency portion of the spectrum, which is an essential requirement to get the source size information from the IPS temporal spectrum as well as inner-scale (i.e., cut-off scale) size of the solar wind turbulence (Manoharan et al 2000). Thus, PONDER will be very useful for the understanding of the smallest scale in solar wind turbulence.

## 5 Summary and Future plans

A new real-time backend, PONDER, designed to operate with the legacy system of the ORT has been described in this paper. PONDER uses current state of the art computing hardware, a GPU board and a large disk storage to support high time resolution real-time pulsar data by employing coherent dedispersion over a bandpass of 16 MHz. Moreover, PONDER can be operated in a variety of observing modes using a GUI. For example, it can essentially support different modes of pulsar observations and each mode leads to standard reduced data products in the form of integrated pulsar profiles and dedispersed time series, which allow a faster turn-around time from observations to scientific results. There is ample scope for getting additional data products in future. In the case of IPS observations, PONDER has demonstrated the improved sensitivity of the fluctuation spectrum at the high-frequency portion of the spectrum, which is important in getting some of the crucial solar-wind parameters. The IPS mode has also enabled the availability of correlated time series and fluctuation spectrum products with high time and frequency resolution in real time. Additionally, the capabilities of PONDER illustrated by the pulsar and IPS modes can be extended to use for a variety of other astrophysical studies possible using the high sensitivity of the ORT.

In the near future, it is proposed to add a dynamic-spectrum mode for pulsar observations to obtain online dynamic spectra as a standard data product for the studies of ISM using pulsars as the probe. Another enhancement will be an automated pipeline using the gated pulsar observations planned in the dynamic spectra mode, to detect nulls and generate estimates of nulling fractions of the pulsars. Lastly, we also plan to add a copy of the backend to other beams of the legacy system, with additional capability of automatic detection of transients, such as fast radio bursts (Thornton et al 2013).

**Acknowledgements** We would like to thank all the staff members of the Radio Astronomy Center for helping us in various stages of the development and testing of the receiver. In particular, we acknowledge the help from D. Nandagopal, K. Kalyanasundaram, Arun E Varghese, Amit Kumar Mittal & G.V.S Girish for helping us with various stages of the PONDER development. We also thank all the operators of the ORT who have assisted during the observations mentioned in the paper mainly V. Magesh, R. Chandrasekhar, P. Praveen & Neville Jude. The ORT is operated and maintained at the Radio Astronomy Centre by the National Centre for Radio Astrophysics of the Tata Institute of Fundamental Research. We are grateful to the anonymous referees for their careful and critical reading of the manuscript and useful comments.

## References

Demorest PB, Ferdman RD, Gonzalez ME, Nice D, Ransom S, Stairs IH, Arzoumanian Z, Brazier A, Burke-Spolaor S, Chamberlin SJ, Cordes JM, Ellis J, Finn LS, Freire P, Giampanis S, Jenet F, Kaspi VM, Lazio J, Lommen AN, McLaughlin M, Palliyaguru N, Perrodin D, Shannon RM, Siemens X, Stinebring D, Swiggum J, Zhu WW (2013) Limits on the Stochastic Gravitational Wave Background from the North American Nanohertz

- Observatory for Gravitational Waves. *ApJ* 762:94, DOI 10.1088/0004-637X/762/2/94, 1201.6641
- DuPlain R, Ransom S, Demorest P, Brandt P, Ford J, Shelton AL (2008) Launching GUPPI: the Green Bank Ultimate Pulsar Processing Instrument. In: Society of Photo-Optical Instrumentation Engineers (SPIE) Conference Series, Society of Photo-Optical Instrumentation Engineers (SPIE) Conference Series, vol 7019, DOI 10.1117/12.790003
- Foster RS, Backer DC (1990) Constructing a pulsar timing array. *ApJ* 361:300
- Hankins TH (1971) Microsecond Intensity Variations in the Radio Emissions from CP 0950. *ApJ* 169:487, DOI 10.1086/151164
- Hankins TH, Rickett BJ (1975a) Pulsar signal processing. In: *Methods in Computational Physics Volume 14 — Radio Astronomy*, Academic Press, New York, pp 55–129
- Hankins TH, Rickett BJ (1975b) Pulsar signal processing. *Methods in Computational Physics* 14:55–129
- Hankins TH, Kern JS, Weatherall JC, Eilek JA (2003) Nanosecond radio bursts from strong plasma turbulence in the Crab pulsar. *Nature* 422:141–143
- Hobbs GB, Edwards RT, Manchester RN (2006) TEMPO2, a new pulsar-timing package - I. An overview. *MNRAS* 369:655–672, DOI 10.1111/j.1365-2966.2006.10302.x, astro-ph/0603381
- Jenet F, Anderson S, Kaspi V, Prince T, Unwin S (1998) Radio pulse properties of the millisecond pulsar PSR J0437–4715. I. Observations at 20 centimeters. *ApJ* 498:365–372
- Johnston S, Romani R (2002) A search for giant pulses in Vela-like pulsars. *MNRAS* 332:109–115
- Johnston S, Romani R (2003) Giant pulses from psr b0540-69 in the large magellanic cloud. *ApJ* 590:L95–L98
- Joshi BC, Ramakrishna S (2006) A software baseband receiver for pulsar astronomy at GMRT. *Bulletin of the Astronomical Society of India* 34:401, astro-ph/0611331
- Joshi BC, Lyne AG, Kramer M, Lorimer DR, Jordan C, Holloway A, Ikin T, Stairs IH (2003) Coherent On-line Baseband Receiver for Astronomy. In: Bailes M, Nice DJ, Thorsett S (eds) *Radio Pulsars*, Astronomical Society of the Pacific, San Francisco, p 321
- Joshi BC, Kramer M, Lyne AG, McLaughlin MA, Stairs IH (2004) Giant Pulses in Millisecond Pulsars. In: Camilo F, Gaensler BM (eds) *IAU Symposium*, p 319
- Karuppusamy R, Stappers B, van Straten W (2008) PuMa-II: A Wide Band Pulsar Machine for the Westerbork Synthesis Radio Telescope. *Proc Astr Soc Aust* 120:191–202, DOI 10.1086/528699
- Kinkhabwala A, Thorsett SE (2000) Multifrequency observations of giant radio pulses from the millisecond pulsar B1937+21. *ApJ* 535:365–372
- Kramer M (1998) Determination of the geometry of the PSR B1913+16 system by geodetic precession. *ApJ* 509:856–860
- Kramer M, Johnston S, van Straten W (2002) High-resolution single-pulse studies of the Vela pulsar. *MNRAS* 334:523–532
- Kramer M, Stairs IH, Manchester RN, McLaughlin MA, Lyne AG, Ferdman RD, Burgay M, Lorimer DR, Possenti A, D’Amico N, Sarkissian JM, Hobbs GB, Reynolds JE, Freire PCC, Camilo F (2006) Tests of General Relativity from Timing the Double Pulsar. *Science* 314:97–102, DOI 10.1126/science.1132305
- Krishnakumar MA, Mitra D, Naidu A, Joshi BC, Manoharan PK (2015) Scatter broadening measurements of 124 pulsars at 327 MHz. *ArXiv e-prints* 1501.05401
- Lorimer DR (2001) SIGPROC-v1.0: (Pulsar) Signal Processing Programs, Arecibo Technical Memo No. 2001–01
- Lundgren SC, Cordes JM, Ulmer M, Matz SM, Lomatch S, Foster RS, Hankins T (1995) Giant pulses from the crab pulsar: A joint radio and gamma-ray study. *ApJ* 453:433–445
- Lyne AG, Burgay M, Kramer M, Possenti A, Manchester RN, Camilo F, McLaughlin MA, Lorimer DR, D’Amico N, Joshi BC, Reynolds J, Freire PCC (2004) A double-pulsar system: A rare laboratory for relativistic gravity and plasma physics. *Science* 303:1153–1157
- Manchester RN, Hobbs G, Bailes M, Coles WA, van Straten W, Keith MJ, Shannon RM, Bhat NDR, Brown A, Burke-Spolaor SG, Champion DJ, Chaudhary A, Edwards RT, Hampson G, Hotan AW, Jameson A, Jenet FA, Kesteven MJ, Khoo J, Kocz J, Maciesiak

- K, Osłowski S, Ravi V, Reynolds JR, Sarkissian JM, Verbiest JPW, Wen ZL, Wilson WE, Yardley D, Yan WM, You XP (2013) The Parkes Pulsar Timing Array Project. *Proc Astr Soc Aust* 30:e017, DOI 10.1017/pasa.2012.017, 1210.6130
- Manoharan PK (2012) Three-dimensional Evolution of Solar Wind during Solar Cycles 22-24. *ApJ* 751:128, DOI 10.1088/0004-637X/751/2/128, 1203.6715
- Manoharan PK, Kojima M, Gopalswamy N, Kondo T, Smith Z (2000) Radial Evolution and Turbulence Characteristics of a Coronal Mass Ejection. *ApJ* 530:1061–1070, DOI 10.1086/308378
- Manoharan PK, Tokumaru M, Pick M, Subramanian P, Ipavich FM, Schenk K, Kaiser ML, Lepping RP, Vourlidas A (2001) Coronal Mass Ejection of 2000 July 14 Flare Event: Imaging from Near-Sun to Earth Environment. *ApJ* 559:1180–1189, DOI 10.1086/322332
- Popov MV, Bartel N, Cannon WH, Novikov AY, Kondratiev VI, Altunin VI (2002) Pulsar microstructure and its quasi-periodicities with the s2 vlbi system at a resolution of 62.5 nanoseconds. *A&A* pp 171–187
- Romani RW, Narayan R, Blandford R (1986) Refractive effects in pulsar scintillation. *MNRAS* 220:19–49
- Sallmen S, Backer DC (1995) Single pulse statistics for PSR 1534+12 and PSR 1937+21. In: Fruchter AS, Tavani M, Backer DC (eds) *Millisecond Pulsars: A Decade of Surprise*, *Astron. Soc. Pac. Conf. Ser. Vol. 72*, pp 340–342
- van Straten W, Bailes M, Britton M, Kulkarni SR, Anderson SB, Manchester RN, Sarkissian J (2001) A test of general relativity from the three-dimensional orbital geometry of a binary pulsar. *Nature* 412:158–160
- Swarup G, Sarma NVG, Joshi MN, Kapahi VK, Bagri DS, Damle SH, Ananthakrishnan S, Balasubramanian V, Bhawe SS, Sinha RP (1971) Large Steerable Radio Telescope at Ootacamund, India. *Nature Physical Science* 230:185–188, DOI 10.1038/physci230185a0
- Taylor JH, Weisberg JM (1989) Further experimental tests of relativistic gravity using the binary pulsar PSR 1913+16. *ApJ* 345:434–450
- Thornton D, Stappers B, Bailes M, Barsdell B, Bates S, Bhat NDR, Burgay M, Burke-Spolaor S, Champion DJ, Coster P, D’Amico N, Jameson A, Johnston S, Keith M, Kramer M, Levin L, Milia S, Ng C, Possenti A, van Straten W (2013) A Population of Fast Radio Bursts at Cosmological Distances. *Science* 341:53–56, DOI 10.1126/science.1236789, 1307.1628
- Weisberg JM, Taylor JH (2002) General Relativistic Geodetic Spin Precession in Binary Pulsar B1913+16: Mapping the Emission Beam in Two Dimensions. *ApJ* 576:942–949